

## Supporting Information

### *Modeling the Roles of Rigidity and Dopants in Single-Atom Methane-to-Methanol Catalysts*

Haojun Jia<sup>1,2</sup>, Aditya Nandy<sup>1,2</sup>, Mingjie Liu<sup>1</sup>, and Heather J. Kulik<sup>1,\*</sup>

<sup>1</sup>Department of Chemical Engineering, Massachusetts Institute of Technology, Cambridge, MA 02139

<sup>2</sup>Department of Chemistry, Massachusetts Institute of Technology, Cambridge, MA 02139

#### Contents

<b>Figure S1</b> SAC model construction	Page S2
<b>Table S1</b> Total energies for LS and IS SACs and intermediates	Page S2
<b>Table S2</b> Spin splitting energies for LS and IS SACs	Page S2
<b>Table S3</b> Reaction energies for LS and IS SACs	Page S3
<b>Table S4</b> Spin states and charges of all compounds in this work	Page S3
<b>Figure S2</b> Structures of increasingly large SAC models	Page S4
<b>Figure S3</b> Center of mass differences between initial and final SACs by dopant and size	Page S4
<b>Table S5</b> Center of mass differences between initial and final SACs by dopant and size	Page S5
<b>Figure S4</b> Metal-local RMSD measured by metal and four metal-coordinating atoms	Page S5
<b>Table S6</b> Metal–ligand bond lengths of SACs by dopant and size	Page S5
<b>Figure S5</b> Distortion in P- and S-coordinating SACs	Page S6
<b>Table S7</b> Metal–ligand bond lengths of SACs, macrocycles, and TMCs	Page S6
<b>Figure S6</b> Catalytic intermediates of N- and O-coordinating SACs	Page S7
<b>Table S8</b> Primary coordination sphere dopant–dopant distances of SACs	Page S8
<b>Table S9</b> Covalent radii of Fe–X bonds used for relative bond lengths	Page S8
<b>Table S10</b> Relative metal–ligand bond lengths of all compounds	Page S9
<b>Table S11</b> Complexation energies of SACs with and without constraints	Page S10
<b>Table S12</b> Mulliken spin density on intermediates in representative SACs	Page S10
<b>Table S13</b> NBO analysis of resting state catalyst SAC metal center charges	Page S10
<b>Table S14</b> Oxo formation energetics on non-metal sites of SACs	Page S11
<b>Figure S7</b> Scatter plot of $\omega$ PBEh and B3LYP calculations on SACs	Page S11
<b>Figure S8</b> Parity plot of $\omega$ PBEh and B3LYP calculations on SACs by reaction energy	Page S12
<b>Figure S9</b> Scatter plot of SQ complexes with multiple ligand types	Page S13
<b>Figure S10</b> Scatter plot of SQ complexes with a single ligand type	Page S14
<b>Figure S11</b> KDE plot of reaction energetics on TE complexes compared to SACs	Page S15
<b>Figure S12</b> KDE plot of reaction energetics on SQ and TE complexes	Page S16
<b>Figure S13</b> Scatter plot of reaction energetics on TE complexes	Page S17
<b>Figure S14</b> Catalytic intermediates of N- and P-coordinating macrocycles	Page S18
<b>Figure S15</b> The last cycle of NEB for the oxo formation transition state	Page S19
<b>Figure S16</b> The bond length scan between O and H for the HAT transition state	Page S20
<b>References</b>	Page S20

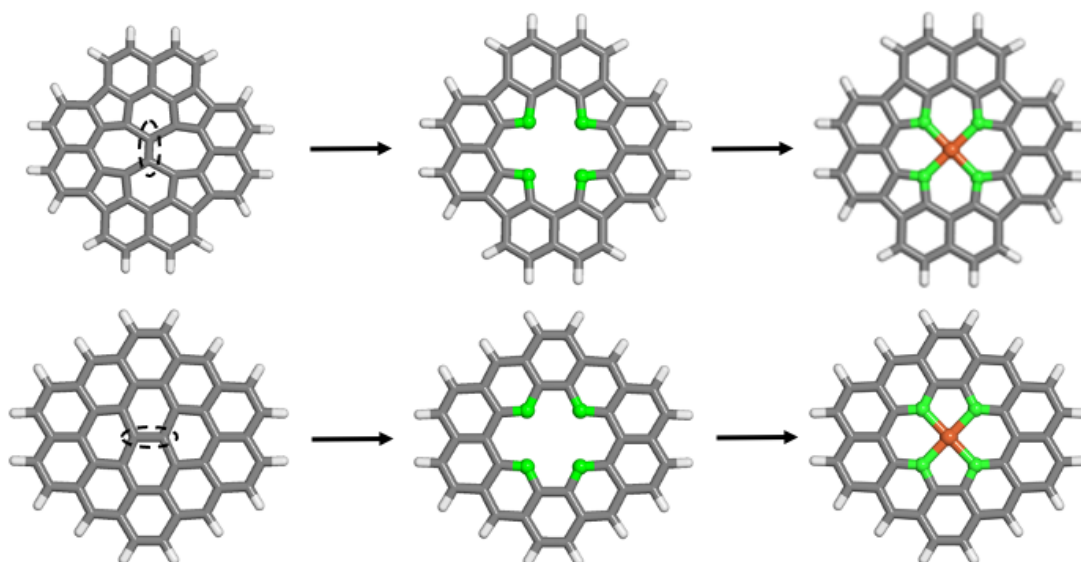


**Figure S1.** Creation of a divacancy in 5- and 6-membered ring graphene flakes (top and bottom respectively). The two carbon atoms annotated with a dashed circle are removed to create a vacancy (left). The four nearest carbon atoms to this region are replaced by dopant atoms (middle). Finally, the Fe atom is embedded in the middle of the divacancy to complete the SAC model (right).

**Table S1.** Total energies (in Ha) for LS and IS N-doped 5- and 6-membered ring SACs and intermediates.

system	spin state	resting state energy (Ha)	oxo energy (Ha)	hydroxyl energy (Ha)	methanol energy (Ha)
5-membered Fe-N-C	LS	-1874.8439	-1949.9342	-1950.6178	-1990.4720
	IS	-1874.9148	-1949.9961	-1950.6391	-1990.5272
6-membered Fe-N-C	LS	-1721.9736	-1797.0657	-1797.7547	-1837.6396
	IS	-1722.0352	-1797.1170	-1797.7630	-1837.5627

**Table S2.** Spin splitting energy (in kcal/mol) for LS and IS N-doped 5- and 6-membered ring SACs.

system	$\Delta E_{I-L}$ spin splitting energy (kcal/mol)			
	resting state	oxo	hydroxyl	methanol
5-membered Fe-N-C	-44.49	-38.87	-13.35	-34.68
6-membered Fe-N-C	-38.63	-32.19	-5.21	-38.63

**Table S3.** Reaction energetics (in kcal/mol) for LS and IS N-doped 5- and 6-membered ring SACs.

system	spin state	$\Delta E(\text{oxo})$ (kcal/mol)	$\Delta E(\text{HAT})$ (kcal/mol)	$\Delta E(\text{rebound})$ (kcal/mol)	$\Delta E(\text{release})$ (kcal/mol)
5-membered Fe-N-C	LS	-12.69	-3.42	-39.76	19.02
	IS	-7.07	22.09	-61.09	9.21
6-membered Fe-N-C	LS	-13.83	-6.79	-59.05	42.81
	IS	-7.30	20.17	-72.82	23.17

**Table S4.** Spin states and charges for 5- and 6-membered ring SAC models, 14-membered macrocyclic Fe complexes, and transition-metal complexes with different coordinating atoms (N, O, P and S). For all SAC models, the spin states of other catalytic intermediates are also indicated. Systems that were not explicitly studied in this work are indicated with "--". In all instances, we treat iron as Fe(II) and add it with a net charge of +2.

system	resting state spin state	metal oxo spin state	metal hydroxyl spin state	metal methanol spin state	system charge
<b>5-membered ring SAC</b>					
Fe-N-C	singlet	singlet	doublet	singlet	-2
Fe-O-C	singlet	singlet	doublet	singlet	+2
Fe-P-C	singlet	singlet	doublet	singlet	-2
Fe-S-C	singlet	singlet	doublet	singlet	+2
<b>6-membered ring SAC</b>					
Fe-N-C	singlet	singlet	doublet	singlet	+2
Fe-O-C	singlet	singlet	doublet	singlet	+2
Fe-P-C	singlet	singlet	doublet	singlet	+2
Fe-S-C	singlet	singlet	doublet	singlet	+2
<b>14-membered macrocycle</b>					
Fe-N-C	singlet	--	--	--	+2
Fe-O-C	singlet	--	--	--	+2
Fe-P-C	singlet	--	--	--	+2
Fe-S-C	singlet	--	--	--	+2
<b>TMC</b>					
Fe(pyridine) <sub>6</sub>	singlet	--	--	--	+2
Fe(4H-pyran) <sub>6</sub>	singlet	--	--	--	+2
Fe(phosphinine) <sub>6</sub>	singlet	--	--	--	+2
Fe(4H-thiopyran) <sub>6</sub>	singlet	--	--	--	+2
Fe(pyrrole) <sub>6</sub>	singlet	--	--	--	-4
Fe(furan) <sub>6</sub>	singlet	--	--	--	+2
Fe(phospholide) <sub>6</sub>	singlet	--	--	--	-4
Fe(thiophene) <sub>6</sub>	singlet	--	--	--	+2

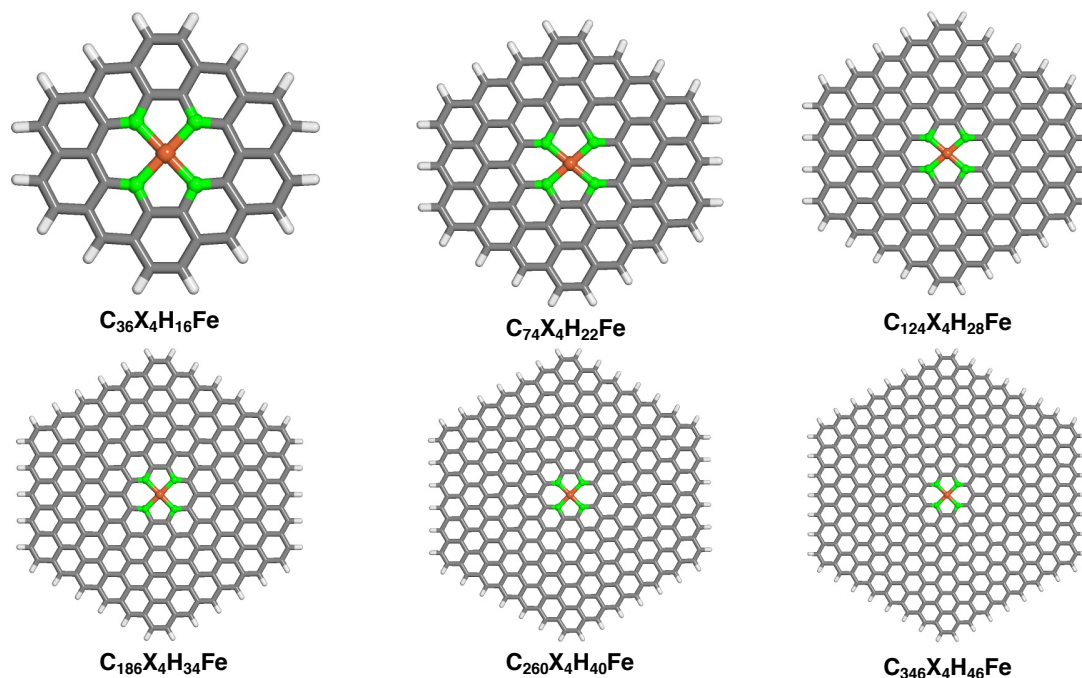


**Figure S2.** Atomic structures of increasingly large SACs with different coordinating atoms shown in green (X = N, O, P or S). The representative structures are shown in ball-and-stick representation colored as follows: Fe in brown, C in gray, and H in white.

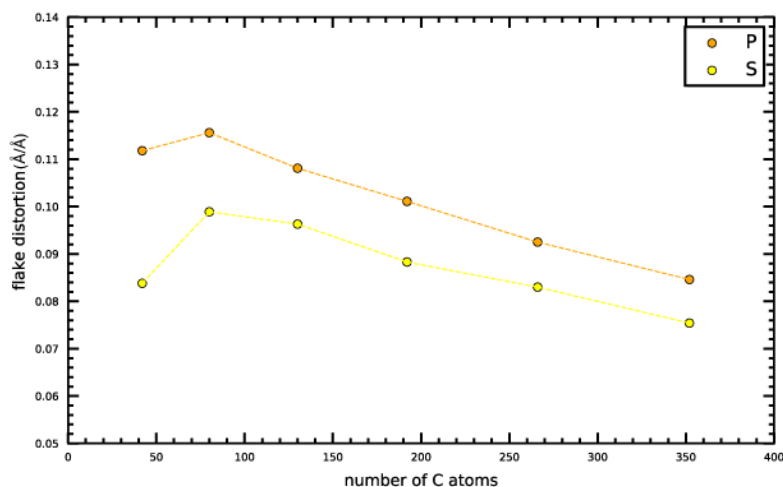


**Figure S3.** Normalized flake distortion of increasingly large P- and S-coordinating SACs with full geometry optimization. Distortion is quantified by measuring the distance of the center of mass from the initial planar SAC geometry after dividing the size of corresponding flake. Here, the number of C atoms refers to all atoms in the flake prior to insertion of the vacancy and placement of the dopants and iron.

**Table S5.** Out-of-plane distortion of increasingly large SACs with P- and S-coordinating atoms for full geometry optimization as quantified by distance of the center of mass from the initial planar SAC geometry. All distances are in units of Å.

system	out-of-plane distortion	out-of-plane distortion
	X=P	X=S
C <sub>36</sub> X <sub>4</sub> H <sub>16</sub> Fe	1.52	1.14
C <sub>74</sub> X <sub>4</sub> H <sub>22</sub> Fe	2.07	1.77
C <sub>124</sub> X <sub>4</sub> H <sub>28</sub> Fe	2.39	2.13
C <sub>186</sub> X <sub>4</sub> H <sub>34</sub> Fe	2.67	2.33
C <sub>260</sub> X <sub>4</sub> H <sub>40</sub> Fe	2.84	2.55
C <sub>346</sub> X <sub>4</sub> H <sub>46</sub> Fe	2.96	2.64

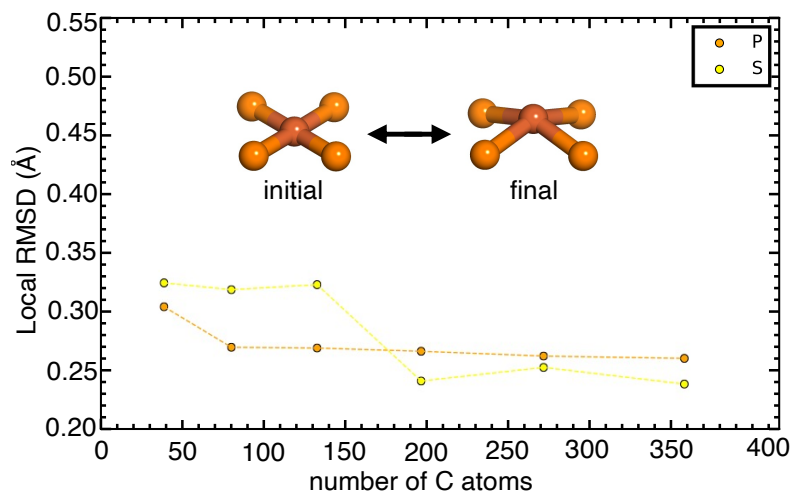


**Figure S4.** Local root-mean-square deviation (RMSD) of the metal and four coordinating atoms of increasingly large P- and S-coordinating SACs as quantified by the difference between the initial planar and the fully optimized distorted structures. Here, the number of C atoms refers to all atoms in the flake prior to insertion of the vacancy and placement of the dopants and iron.

**Table S6.** Average metal–ligand bond lengths of increasingly large SACs with different coordinating atoms (N, O, P and S). All distances are in units of Å.

system	bond length	bond length	bond length	bond length
	X=N	X=O	X=P	X=S
C <sub>36</sub> X <sub>4</sub> H <sub>16</sub> Fe	1.92	1.90	2.15	2.21
C <sub>74</sub> X <sub>4</sub> H <sub>22</sub> Fe	1.90	1.90	2.07	2.10
C <sub>124</sub> X <sub>4</sub> H <sub>28</sub> Fe	1.91	1.89	2.07	2.11
C <sub>186</sub> X <sub>4</sub> H <sub>34</sub> Fe	1.91	1.90	2.07	2.09
C <sub>260</sub> X <sub>4</sub> H <sub>40</sub> Fe	1.88	1.89	2.06	2.10
C <sub>346</sub> X <sub>4</sub> H <sub>46</sub> Fe	1.87	1.90	2.06	2.09

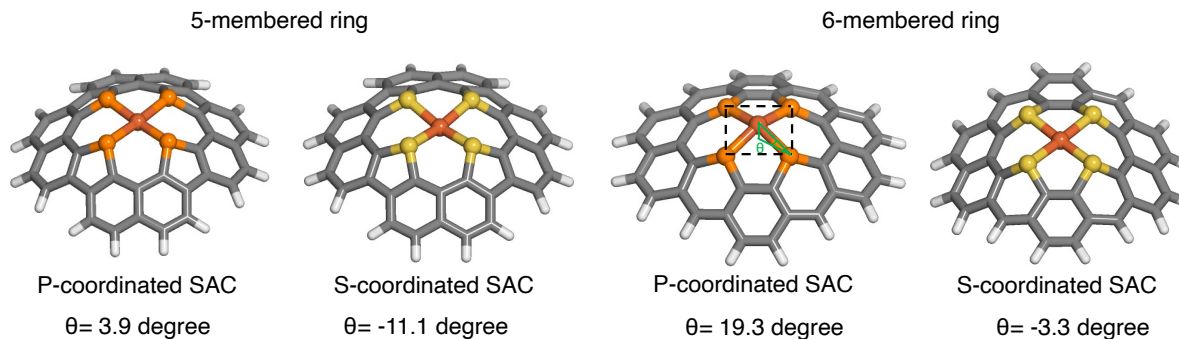


**Figure S5.** The metal dihedral angle,  $\theta$ , is the dihedral angle between the Fe metal and the plane formed by any 3 of the 4 coordinating atoms. This angle is shown schematically in the P-coordinated 5-membered ring SAC. A negative value for this angle indicates that metal lies below the coordinating atom plane.

**Table S7.** Average metal–ligand bond lengths (BLs, in Å) of 5- and 6-membered SAC models, 14-membered macrocyclic complexes, and mononuclear transition-metal complex analogues with and without constraints out of the plane (i.e., the z-axis, for the 5-membered and 6-membered SAC only). Results are shown for cases where all coordinating atoms are one of four elements (N, O, P and S). Systems that were not constrained and have no result are indicated as “--”.

system	full geometry optimization average M-L BL (Å)	constrained z-axis average M-L BL (Å)
<b>5-membered ring SAC</b>		
Fe-N-C	1.97	1.97
Fe-O-C	1.99	1.99
Fe-P-C	2.19	1.95
Fe-S-C	2.15	1.97
<b>6-membered ring SAC</b>		
Fe-N-C	1.92	1.92
Fe-O-C	1.89	1.89
Fe-P-C	2.15	2.01
Fe-S-C	2.21	1.94
<b>14-membered macrocycle</b>		
Fe-N-C	1.84	--
Fe-O-C	1.87	--
Fe-P-C	2.09	--
Fe-S-C	2.13	--
<b>octahedral transition metal complex</b>		
Fe(pyridine) <sub>6</sub>	2.11	--
Fe(4H-pyran) <sub>6</sub>	2.17	--
Fe(phosphinine) <sub>6</sub>	2.25	--
Fe(4H-thiopyran) <sub>6</sub>	2.38	--
Fe(pyrrole) <sub>6</sub>	2.11	--
Fe(furan) <sub>6</sub>	2.03	--
Fe(phospholide) <sub>6</sub>	2.33	--
Fe(thiophene) <sub>6</sub>	2.38	--

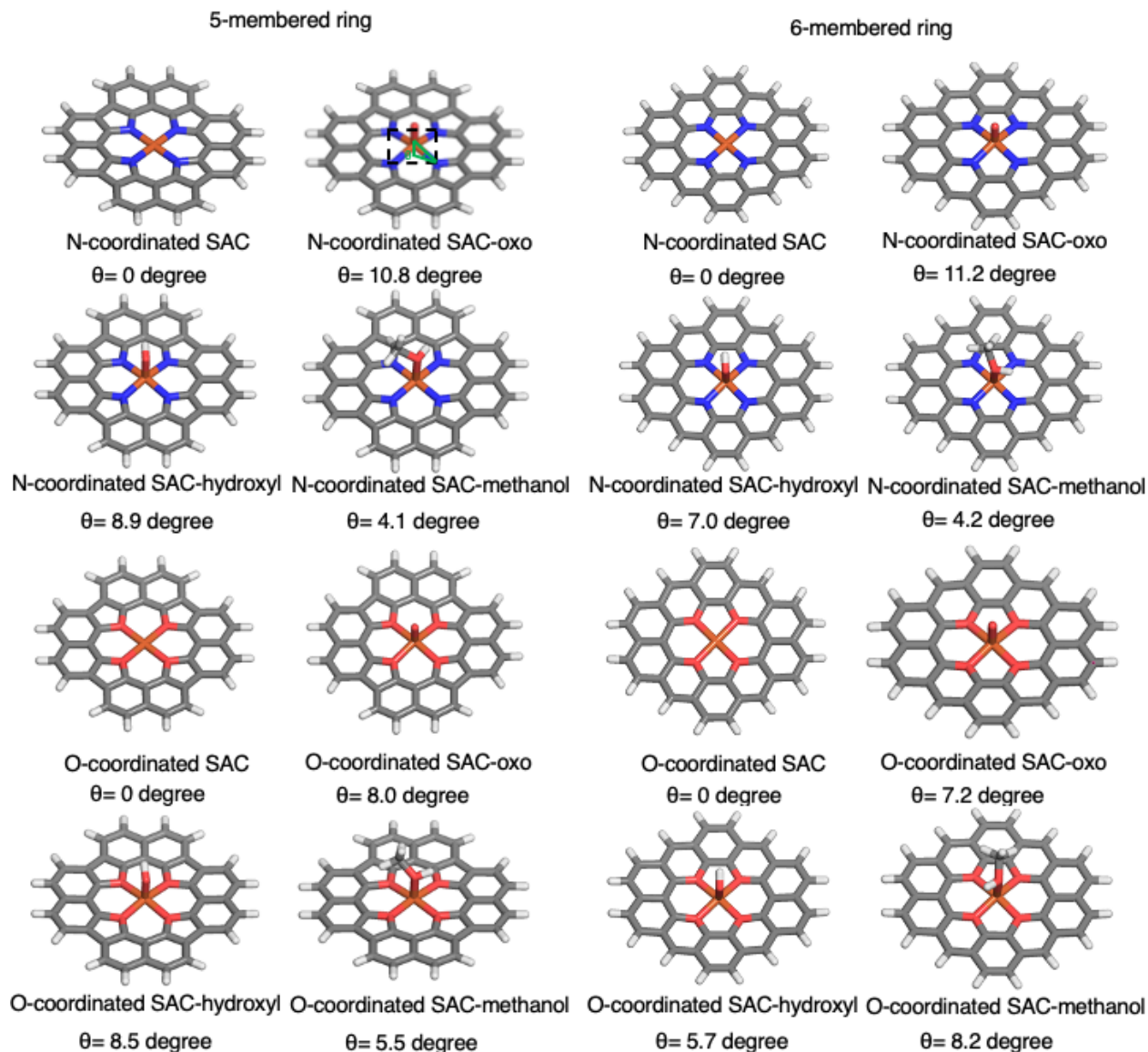


**Figure S6.** The metal dihedral angle,  $\theta$  (labeled on the N-coordinating 5-membered ring oxo intermediate structure), is the dihedral angle between the Fe metal and the plane formed by 3 coordinating atoms. We annotate this angle for each intermediate (resting state, oxo, hydroxyl, methanol) in the radical rebound mechanism for conversion of methane to methanol.

**Table S8.** The average dopant–dopant distance (in Å) for 5- and 6-membered SAC models with different coordinating atoms (N, O, P and S).

system	dopant-dopant distance (Å)
<b>5-membered ring SAC</b>	
Fe-N-C	2.80
Fe-O-C	2.80
Fe-P-C	3.10
Fe-S-C	3.11
<b>6-membered ring SAC</b>	
Fe-N-C	2.63
Fe-O-C	2.78
Fe-P-C	2.95
Fe-S-C	3.13

**Table S9.** Covalent radii of X bonds (in Å). The low-spin (LS) Fe covalent radius is estimated to be 1.42 Å<sup>1</sup>.

X	X radius (Å)
N	0.71
O	0.66
P	1.07
S	1.05

**Table S10.** Relative metal–ligand bond length,  $d_{\text{rel}}(\text{Fe-X})$ , of 5- and 6-membered ring SAC models, 14-membered macrocyclic Fe complexes and mononuclear transition-metal complex analogues with different coordinating atoms (N, O, P and S). All relative bond lengths are unitless because they are the ratios of the bond length to the sum of the covalent radii of the substituent atoms.

system	$d_{\text{rel}}(\text{Fe-X})$
<b>5-membered ring SAC</b>	
Fe-N-C	0.93
Fe-O-C	0.95
Fe-P-C	0.88
Fe-S-C	0.87
<b>6-membered ring SAC</b>	
Fe-N-C	0.90
Fe-O-C	0.91
Fe-P-C	0.87
Fe-S-C	0.89
<b>14-membered macrocycle</b>	
Fe-N-C	0.86
Fe-O-C	0.90
Fe-P-C	0.84
Fe-S-C	0.86
<b>octahedral transition metal complex</b>	
Fe(pyridine) <sub>6</sub>	0.99
Fe(4H-pyran) <sub>6</sub>	1.04
Fe(phosphinine) <sub>6</sub>	0.90
Fe(4H-thiopyran) <sub>6</sub>	0.96
Fe(pyrrole) <sub>6</sub>	0.99
Fe(furan) <sub>6</sub>	0.97
Fe(phospholide) <sub>6</sub>	0.94
Fe(thiophene) <sub>6</sub>	0.96

**Table S11.** Complexation energies (in eV) of 5- and 6-membered ring SAC models and 14-membered macrocyclic Fe complexes with different coordinating atoms (N, O, P and S) and constraint conditions.

system	full geometry optimization complexation energy (eV)	constrained z-axis complexation energy (eV)	difference between full and constrained (eV)
<b>5-membered ring SAC</b>			
Fe-N-C	-38.08	-38.09	0.01
Fe-O-C	-31.18	-31.18	0.00
Fe-P-C	-33.54	-32.17	-1.37
Fe-S-C	-32.63	-32.03	-0.60
<b>6-membered ring SAC</b>			
Fe-N-C	-37.37	-37.58	0.20
Fe-O-C	-28.60	-28.75	0.14
Fe-P-C	-33.64	-32.10	-1.54
Fe-S-C	-31.39	-29.84	-1.55
<b>14-membered macrocycle</b>			
Fe-N-C	-38.24	--	--
Fe-O-C	-28.10	--	--
Fe-P-C	-33.39	--	--
Fe-S-C	-29.14	--	--

**Table S12.** Comparison of Mulliken spin density on the metal for each intermediate.

system	resting state Mulliken spin density	metal oxo Mulliken spin density	metal hydroxyl Mulliken spin density	metal methanol Mulliken spin density
<b>5-membered ring SAC</b>				
Fe-N-C	0.00	0.00	0.989	0.00
Fe-O-C	0.00	0.00	0.814	0.00
Fe-P-C	0.00	0.00	0.975	0.00
Fe-S-C	0.00	0.00	0.893	0.00
<b>6-membered ring SAC</b>				
Fe-N-C	0.00	0.00	0.952	0.00
Fe-O-C	0.00	0.00	1.034	0.00
Fe-P-C	0.00	0.00	0.955	0.00
Fe-S-C	0.00	0.00	0.986	0.00

**Table S13.** The natural charges and Fe 3d orbital populations for 5- and 6-membered SACs with different coordinating atoms (N, O, P and S).

system	natural charge	NBO 3d orbital population
<b>5-membered ring SACs</b>		
Fe-N-C	0.87457	6.74
Fe-O-C	0.98444	6.64
Fe-P-C	0.35333	7.26
Fe-S-C	0.59156	7.07
<b>6-membered ring SACs</b>		
Fe-N-C	1.03059	6.71
Fe-O-C	0.56377	7.05
Fe-P-C	0.36083	7.24
Fe-S-C	0.58992	7.07

**Table S14.** The flake oxidation energy (in eV) (i.e., the energy for oxo formation) for 5- and 6-membered flakes with different coordinating atoms (N, O, P and S) and no metal present. The favorable oxo formation on the P-containing flake is due to formation of a  $\mu$ -oxo that cannot form when a metal is present. All other oxidation energies are less favorable than the equivalent metal-oxo formation.

system	flake oxidation energy (eV)
<b>5-membered ring flakes</b>	
N-C	-0.40
O-C	2.95
P-C	-2.61
S-C	-0.23
<b>6-membered ring flakes</b>	
N-C	0.52
O-C	2.50
P-C	-5.77
S-C	-0.62

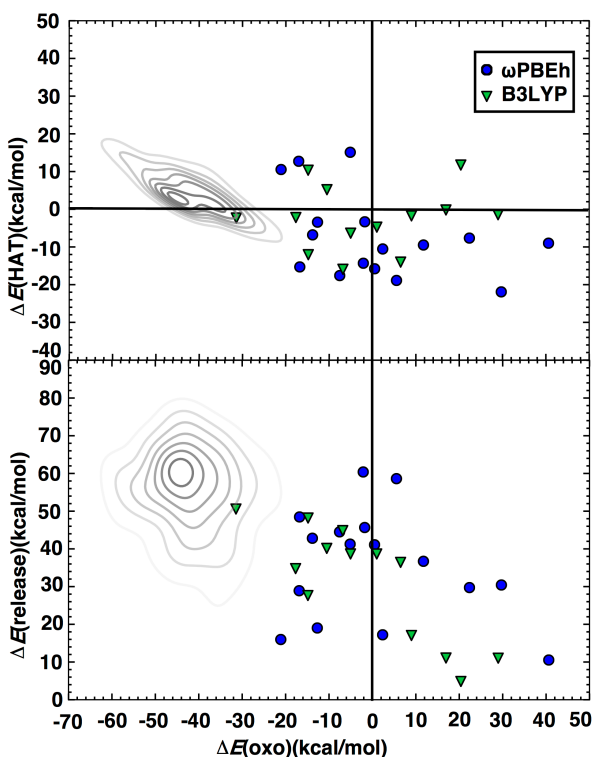


**Figure S7.**  $\Delta E(\text{oxo})$  vs  $\Delta E(\text{HAT})$  (top) and  $\Delta E(\text{oxo})$  vs  $\Delta E(\text{release})$  (bottom) reaction energies (in kcal/mol) of representative TMCs from prior work<sup>2</sup> computed with B3LYP/LACVP\* compared to SAC reaction energies computed with  $\omega\text{PBEh}/\text{LACVP}^*$ , as reported in the main text, (circles) and B3LYP/LACVP\* single-point energies (triangles) on the SAC models. For a subset of O-, P- and S-doped SACs in this work, the B3LYP single-point energy calculations did not converge. The TMCs from prior work are the full LS Fe(II) subset from the square pyramidal constrained (SQ) set of Ref. 2. The TMC KDEs are colored in gray and shown as contour lines with decreasing saturation in 7 evenly spaced levels. Although a different functional is employed, the energy range sampled on SACs is comparable with changing functional.

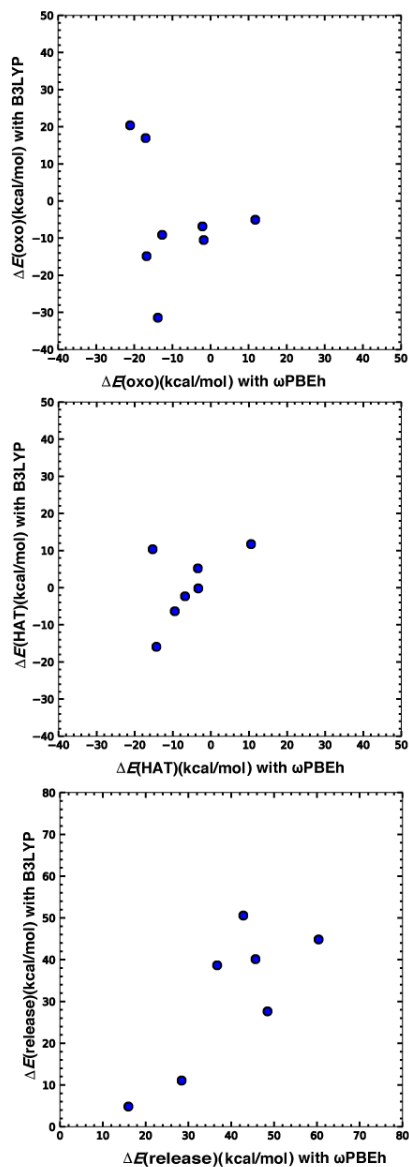


**Figure S8.** Parity plot of SAC reaction energies ( $\Delta E(\text{oxo})$ ,  $\Delta E(\text{HAT})$ ) and  $\Delta E(\text{release})$  between the  $\omega$ PBEh and B3LYP functionals with the LACVP\* basis set in kcal/mol. The B3LYP/LACVP\* energies are evaluated as single-point energies on the  $\omega$ PBEh structures.

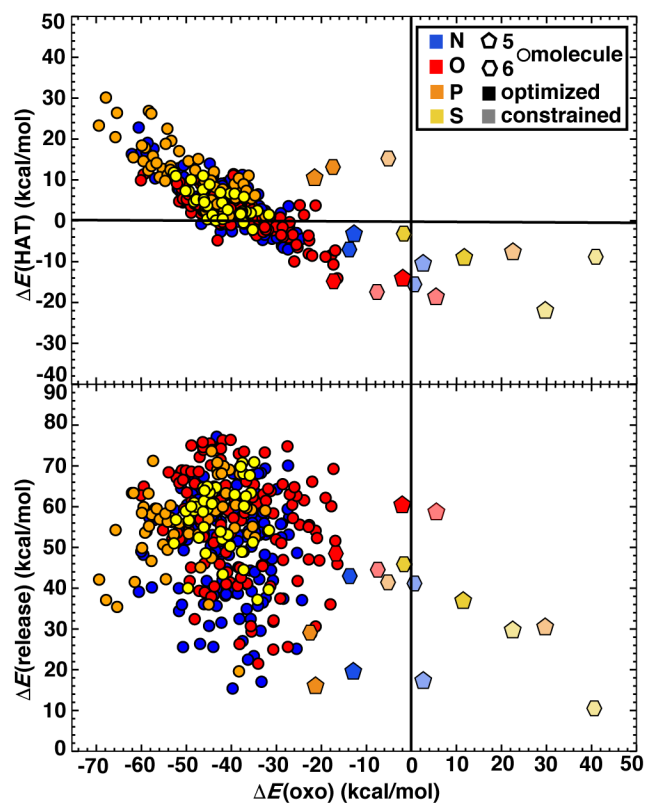


**Figure S9.**  $\Delta E(\text{oxo})$  vs  $\Delta E(\text{HAT})$  (top) and  $\Delta E(\text{oxo})$  vs  $\Delta E(\text{release})$  (bottom) reaction energies (in kcal/mol) of representative transition-metal complexes (TMCs) from prior work<sup>2</sup> compared to 5- (pentagon symbols) and 6-membered (hexagon symbols) ring SAC systems. Both TMCs and SACs are colored by the metal-coordinating atoms in the ligands, as indicated in inset legend. The TMCs are from the all LS Fe(II) in the square pyramidal constrained (SQ) set in Ref. 2. For the complexes containing multiple coordinating atom elements, the symbol is colored by the heavier coordinating atom. The SACs are further distinguished by full geometry optimization (opaque) and constrained z-axis optimization (translucent).

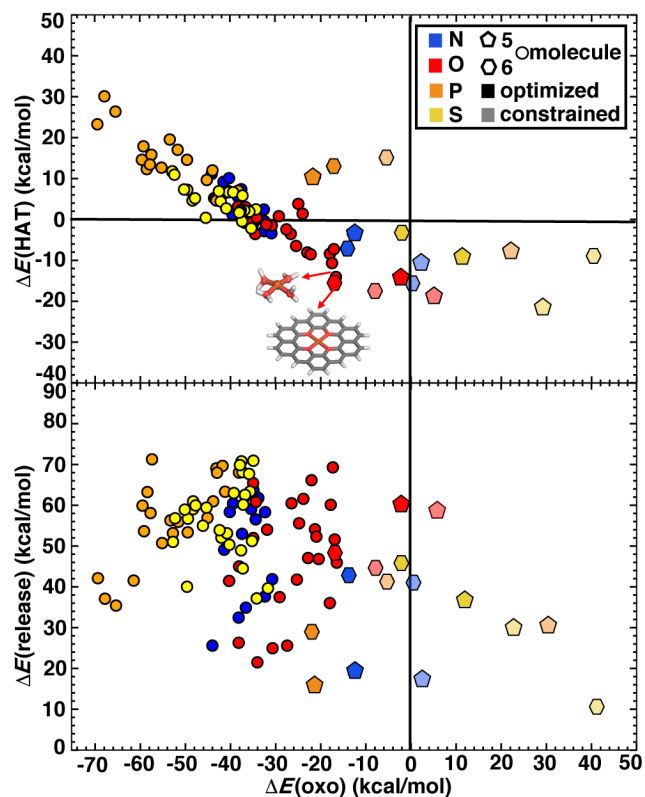


**Figure S10.**  $\Delta E(\text{oxo})$  vs  $\Delta E(\text{HAT})$  (top) and  $\Delta E(\text{oxo})$  vs  $\Delta E(\text{release})$  (bottom) reaction energies (in kcal/mol) of 80 homoleptic LS Fe(II) molecular complexes from the SQ data set in Ref.<sup>2</sup> relative to 5- (pentagon) and 6-membered (hexagon) ring SAC systems. Both TMCs and SACs are colored by metal-coordinating atoms as indicated in inset legend. The TMCs are from the all LS Fe(II) in the square pyramidal constrained (SQ) set in Ref. 2. Representative structures of a O-doped 6-membered ring graphene flake SAC with bond length of 1.9 Å and Fe(II)(OH<sub>2</sub>)<sub>4</sub>-oxo with an out-of-plane distortion angle of 10° and bond length of 2.2 Å are shown in inset. The SACs are further distinguished by full geometry optimization (opaque) and constrained z-axis optimization (translucent).

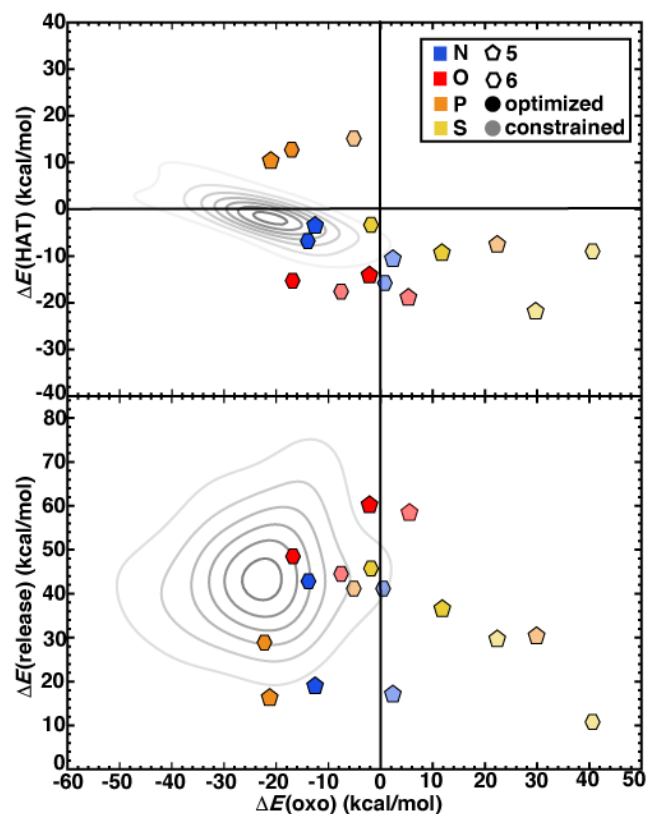


**Figure S11.**  $\Delta E(\text{oxo})$  vs  $\Delta E(\text{HAT})$  (top) and  $\Delta E(\text{oxo})$  vs  $\Delta E(\text{release})$  (bottom) reaction energies (in kcal/mol) of representative TMCs from prior work<sup>2</sup> compared to 5- (pentagon symbols) and 6-membered (hexagon symbols) ring SAC systems. The SACs are colored by the metal-coordinating atoms in the ligands, as indicated in inset legend. The TMCs are from the all LS Fe(II) in the tetragonal equilibrium (TE) set in Ref. 2. The TMCs KDEs are colored in gray and shown as contour lines with decreasing saturation in 7 evenly spaced levels. The SACs are distinguished by full geometry optimization (opaque) and constrained z-axis optimization (translucent).

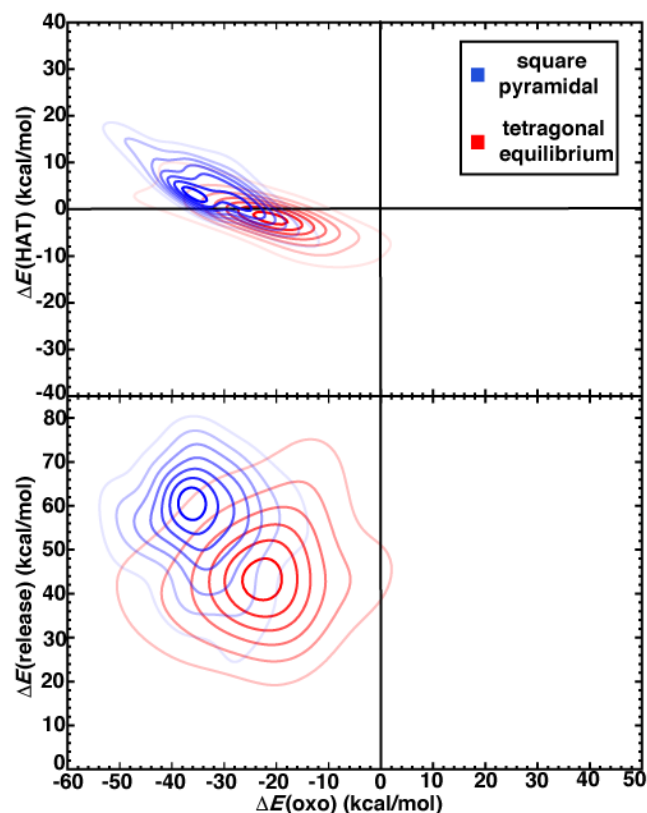


**Figure S12.**  $\Delta E(\text{oxo})$  vs  $\Delta E(\text{HAT})$  (top) and  $\Delta E(\text{oxo})$  vs  $\Delta E(\text{release})$  (bottom) reaction energies (in kcal/mol) for representative TMCs from prior work<sup>2</sup>. The TMCs are from the all LS Fe(II) in the tetragonal equilibrium (TE) and square pyramidal (SQ) set in Ref. 2. The TE and SQ TMC KDEs are colored in red and blue, respectively, and shown as contour lines with decreasing saturation in 7 evenly spaced levels.

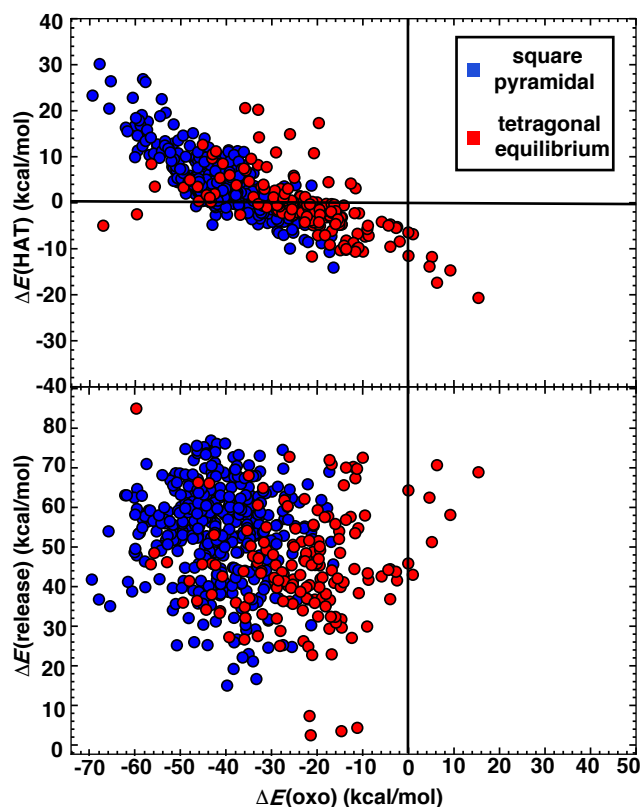


**Figure S13.**  $\Delta E(\text{oxo})$  vs  $\Delta E(\text{HAT})$  (top) and  $\Delta E(\text{oxo})$  vs  $\Delta E(\text{release})$  (bottom) reaction energies (in kcal/mol) of representative TMCs from prior work<sup>2</sup>. The TMCs are from the all LS Fe(II) in the tetragonal equilibrium (TE) and square pyramidal (SQ) set in Ref. 2. The TE and SQ TMC scatters are colored in red and blue, respectively. To show structure in the data, the y-axis scale has been slightly truncated in a manner that excludes four points from LS Fe(II) complexes in the TE set (in red) with very high release values.

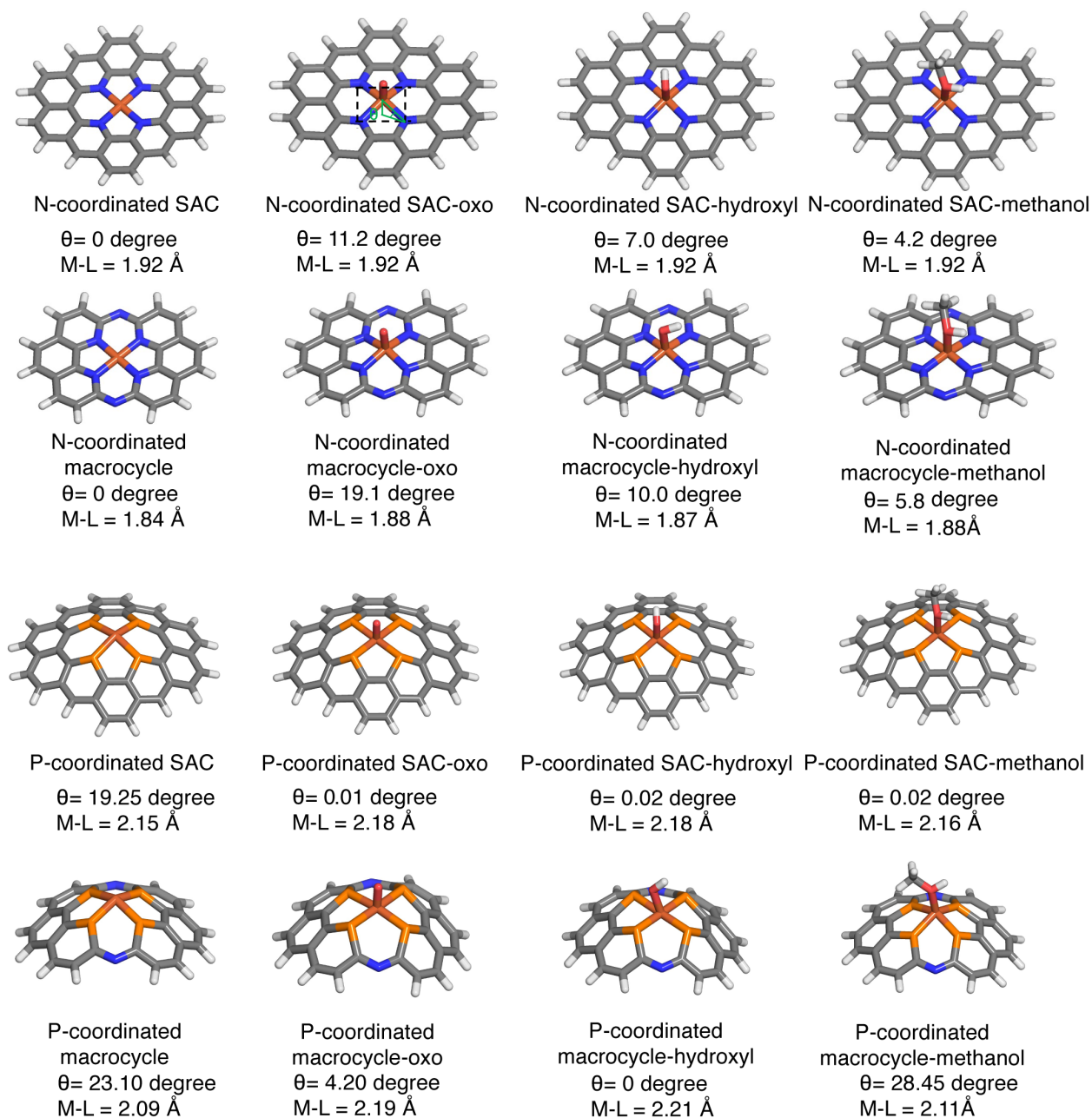


**Figure S14.** The metal dihedral angle,  $\theta$  (labeled on the the N-coordinating SAC oxo intermediate structure), is the dihedral angle between the Fe metal and the plane formed by 3 coordinating atoms. We report this angle for each intermediate (resting state, oxo, hydroxo, methanol) in the radical rebound mechanism for methane-to-methanol conversion.

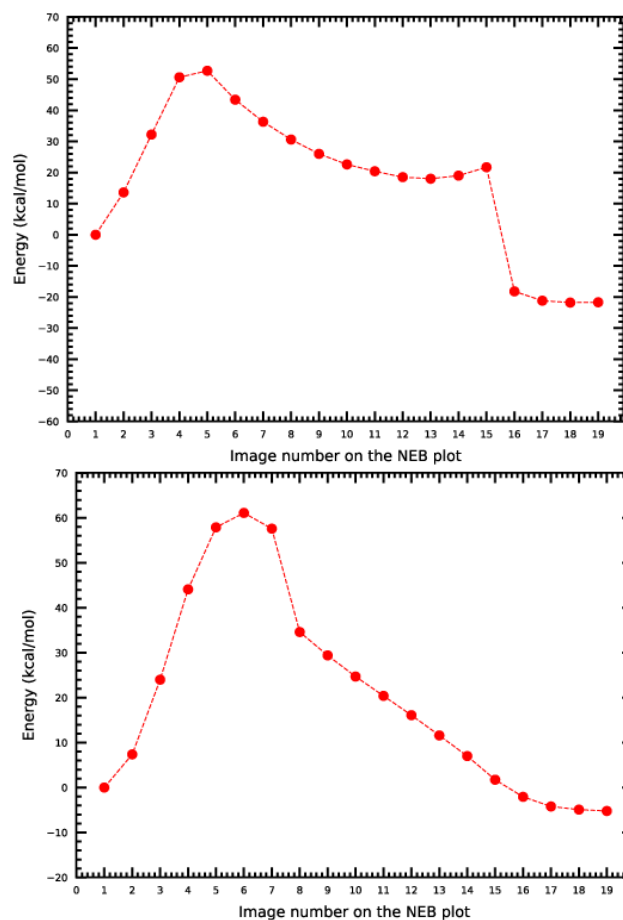


**Figure S15.** The last cycle of Nudged Elastic Band (NEB) in TeraChem ( $\omega$ PBEh/LACVP\*) for oxo formation putative transition states on N-doped 5- and 6-membered ring SACs (top and bottom respectively).

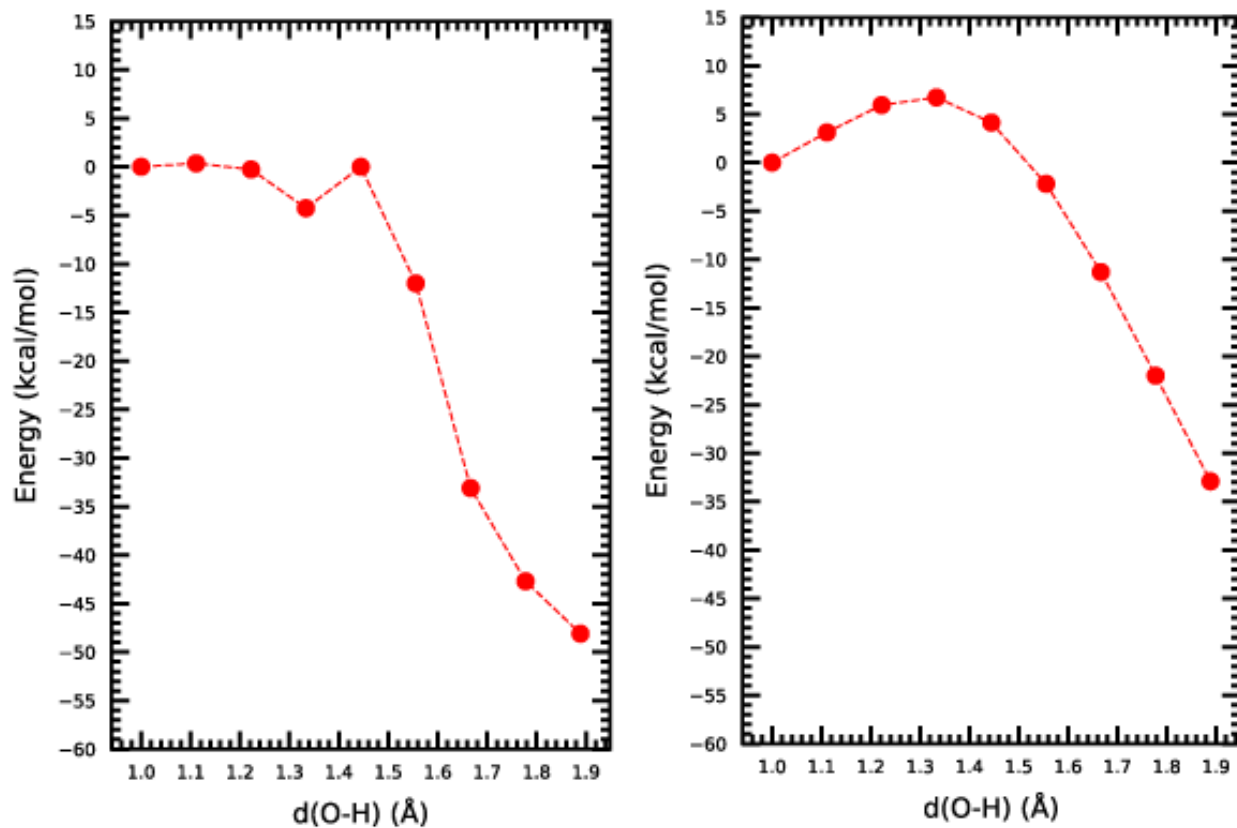


**Figure S16.** The bond length scan between O and H during hydrogen atom transfer (HAT) on N-doped 5- and 6-membered ring SACs (left and right respectively).

## References

1. B. Cordero, V. Gomez, A. E. Platero-Prats, M. Reves, J. Echeverria, E. Cremades, F. Barragan and S. Alvarez, *Dalton Trans.*, 2008, 2832-2838.
2. A. Nandy and H. J. Kulik, *ACS Catal.*, 2020, **10**, 15033-15047.